The Classical Nucleation Model — Entire Process of Crystal Growth and Application to Chirality Conversion —

Makio Uwaha

Department of Physics, Nagoya University Furo-cho, Chikusa-ku, Nagoya, Japan 464-8602

Abstract. With the use of the classical nucleation model, the passage from the initial stage of nucleation to the final stage of Ostwald ripening is surveyed. Direct numerical integration confirms that, under weak initial supersaturation, the drop of supersaturation occurs with a long delay but the relative drop is deep. For various initial supersaturation, the cluster size distribution approaches the single Lifshits-Slyozov-Wagner form. Based on an analysis of current in the cluster size space, a single variable model to describe the time evolution of supersaturation is proposed. The classical nucleation model is generalized and applied to the problem of chirality conversion with grinding crystals.

Keywords: crystallization, classical nucleation model, Becker-Döring model, Ostwald ripening, chirality conversion, sodium chlorate
PACS: 64.60.qe, 81.10.Aj, 81.10.Dn, 82.20.-w

INTRODUCTION

Crystal growth generally proceeds through three distinct stages: nucleation of small crystal nuclei, growth of nuclei to macroscopic crystals and Ostwald ripening. Various models are used to describe these processes by emphasizing specific aspects of crystal growth. The **classical nucleation model** (CNM) describes the system in terms of the number[1] of clusters of the size l at time t: $n_l(t)$. It is a simplified version of a cluster reaction model (see [1]) and only the monomer reaction is taken into account. The CNM was first formulated by L. Farkas [2] based on the idea of L. Szilard. The exact steady-state solution of the model was provided by Becker and Döring, and the model is often called the Becker-Döring model[3]. By neglecting correlations and collisions of clusters as well as complicated processes of growth at the surface, the CNM provides a systematic description for qualitative change of the system[4]. It is the standard model of nucleation to obtain formation rate of supercritical nuclei (the classical nucleation theory: CNT). The CNM also leads to a mean field description of Ostwald ripening known as the Lifshitz-Slyozov-Wagner(LSW) theory[5, 6], which predicts the asymptotic behavior of the system. These initial and final behaviors have been theoretically studied in detail, but the intermediate behavior is much less understood[7].

In this paper we briefly summarize the standard CNT as a theory of the initial stage of crystal growth, and the LSW theory as that of the final stage. With the help of a numerical integration of CNM, we characterize features of an intermediate stage that connects the two limiting stages and try to provide a simple qualitative view of the whole crystallization process[8]. Finally, we discuss an application of the CNM to the recently discovered chirality conversion by grinding crystals in a solution[9].

THE CLASSICAL NUCLEATION MODEL

The Model

The CNM describes the system in terms of the number $n_l(t)$ of clusters, X_l, which consists of l atoms (or molecules) of X. For the reaction

$$\mathrm{X}_1 + \mathrm{X}_l \leftrightarrow \mathrm{X}_{l+1}, \tag{1}$$

[1] In the present paper we consider a system of unit volume, and $n_l(t)$ is, in fact, a number density. We call, however, $n_l(t)$ the number, for simplicity.

the rate to the right is given by $\sigma_l n_1(t) n_l(t)$, and that to the left is $\lambda_{l+1} n_{l+1}(t)$. The coefficient σ_l is proportional to the surface area $\sim l^{2/3}$ of the cluster X_l. It may be proportional to the thermal velocity of the atoms for the growth in a gas. The decay rate λ_l is also proportional to the surface area of the cluster. For small size clusters, however, the decay rate per unit surface area $\sim \lambda_l / l^{2/3}$ increases due to the Gibbs-Thomson effect. The net growth rate is the current in the cluster size space

$$j_l(t) = \sigma_l n_1(t) n_l(t) - \lambda_{l+1} n_{l+1}(t). \tag{2}$$

Change of the number of clusters $n_l(t)$ is given by the continuity equation in the size space as

$$\frac{\partial n_l(t)}{\partial t} = j_{l-1}(t) - j_l(t). \tag{3}$$

Equation (3) holds for $l \geq 2$, and, for $l = 1$, the number of monomers obeys

$$\frac{\partial n_1(t)}{\partial t} = -2\sigma_1 n_1^2(t) - n_1(t) \sum_{l=2}^{\infty} \sigma_l n_l(t) + 2\lambda_2 n_2(t) + \sum_{l=3}^{\infty} \lambda_l n_l(t). \tag{4}$$

The first term is the formation of dimers and the second term represents the consumption of monomers because of the growth of clusters. The last two terms come from the decay of clusters by emitting monomers. The total number of atoms in the system

$$\sum_{l=1}^{\infty} l n_l(t) = N \tag{5}$$

is conserved.

At saturation equilibrium, chemical potential of the vapor and that of the crystal are the same, and a saturated vapor is in equilibrium with a bulk crystal. That is, for very large l, the impingement rate per unit surface area is the same as the decay rate (evaporation or dissolution rate) per unit surface area. See Fig.1(a). Under the equilibrium condition, only small clusters and a bulk crystal exist in the system, and the equilibrium distribution of clusters is given by

$$n_l^{\rm eq} = n_1^{\rm eq} e^{-G_l^{\rm eq}/k_{\rm B}T} = n_1^{\rm eq} \exp\left[-\bar{\alpha}(l^{2/3} - 1)\right] \tag{6}$$

with

$$\bar{\alpha} = (4\pi)^{1/3} (3\Omega)^{2/3} \frac{\alpha}{k_{\rm B}T}, \tag{7}$$

where Ω is the atomic volume, α the surface free energy density[2]. Note that we have assumed the simple form of surface free energy in (6), and that the excess chemical potential (supersaturation) $\Delta\mu = \mu_{\rm gas} - \mu_{\rm solid}$ vanishes at the saturation equilibrium. The suffix "eq" indicates the unique saturation equilibrium.

For the collision rate coefficient σ_l, we assume a kinetics-limited process in three dimensions and put

$$\sigma_l = a l^{2/3}, \tag{8}$$

where a is a constant proportional to the molecular thermal velocity. Evaluation of the decay rate λ_l including the Gibbs-Thomson effect can be done from the detailed balance condition at saturation equilibrium. Since the two reactions in (1) balance at equilibrium, $j_l^{\rm eq} = 0$, *i.e.*

$$\sigma_l n_1^{\rm eq} n_l^{\rm eq} = \lambda_{l+1} n_{l+1}^{\rm eq}. \tag{9}$$

Thus λ_{l+1} is given by

$$\lambda_{l+1} \;=\; \sigma_l n_1^{\rm eq} \exp\left[\bar{\alpha}(l+1)^{2/3} - \bar{\alpha} l^{2/3}\right]. \tag{10}$$

---

[2] $G_l^{\rm eq} = 4\pi R^2 \alpha$ and $(4\pi/3)R^3 = l\Omega$.

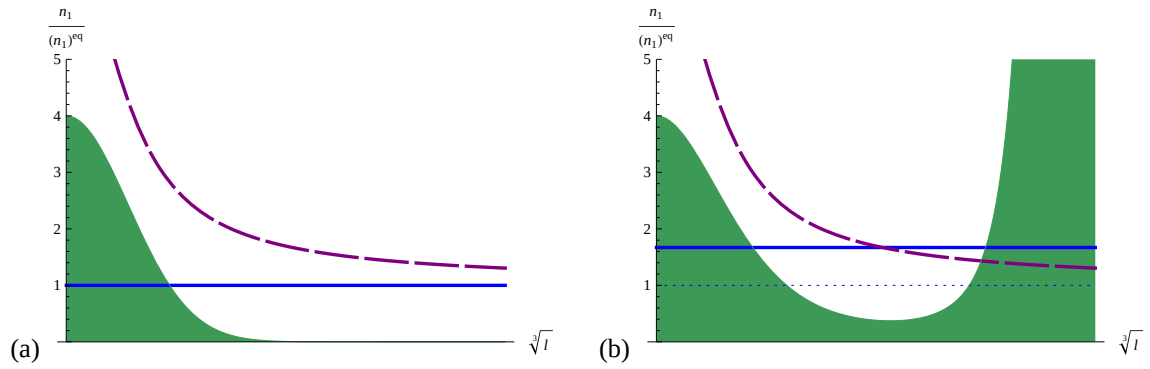

FIGURE 1. Normalized impingement rate (solid blue line) and evaporation (dissolution) rate (dashed purple line) per unit area of the cluster surface vs. the linear size $l^{1/3}$ of the cluster: (a) at saturation equilibrium ($n_1 = n_1^{\rm eq}$), (b) in supersaturated environment ($n_1 > n_1^{\rm eq}$). The shaded areas represent the equilibrium size distributions $n_l^{\rm eq}$ in (a), and the imaginary equilibrium distribution $\bar{n}_l$ in (b), in an arbitrary scale.

For large l, this formula is approximated by

$$\lambda_{l+1} = a l^{2/3} n_1^{\rm eq} \left(1 + \frac{2\bar{\alpha}}{3} \frac{1}{l^{1/3}} \right). \tag{11}$$

In the following numerical calculation, we use the form (11), even for a small l. This choice makes theoretical analysis in the ripening stage simpler, and the corresponding free energy barrier for nucleation is much smaller than the original form (10) so that nucleation process is realized more easily in the numerical calculation.

Undersaturated and Supersaturated States

In Fig.1 we show the impingement rate and the evaporation rate as functions of the cluster size $l^{1/3}$. At saturation equilibrium (Fig.1(a)), the impingement rate per unit surface area is constant ($an_1^{\rm eq}$) and normalized to unity. The evaporation rate (or dissolution rate) per unit area is the same constant for large clusters ($l \to \infty$) and larger for small clusters due to the Gibbs-Thomson effect. Therefore all clusters tend to shrink, and only small clusters exist in the system as the shaded area indicates[3]. This is the saturated equilibrium size distribution $n_l^{\rm eq}$ given by (6).

If the monomer density is smaller than $n_l^{\rm eq}$, the number of clusters decrease compared with $n_l^{\rm eq}$. This is undersaturated equilibrium state, and the cluster size distribution $\bar{n}_l$ is determined by the same condition as the saturation equilibrium, *i.e.* $j_l = 0$:

$$\sigma_l n_1 \bar{n}_l = \lambda_{l+1} \bar{n}_{l+1} \tag{12}$$

with $n_1 < n_1^{\rm eq}$. From (12), the distribution is given by

$$\bar{n}_l = n_1^l \frac{\sigma_1 \sigma_2 \cdots \sigma_{l-1}}{\lambda_2 \lambda_3 \cdots \lambda_l} = \left(\frac{n_1}{n_1^{\rm eq}} \right)^l n_l^{\rm eq}. \tag{13}$$

With the use of the excess chemical potential $\Delta\mu$ compared to the saturation equilibrium[4],

$$\Delta\mu = k_{\rm B} T \ln \frac{n_1}{n_1^{\rm eq}}, \tag{14}$$

the steady distribution is expressed as

$$\bar{n}_l = e^{l\Delta\mu/k_{\rm B}T} n_l^{\rm eq} = n_1 \exp\left(-\frac{G_l}{k_{\rm B}T} \right) \tag{15}$$

---

[3] The graphs are not correct for very small l since the model free energy $G_l^{\rm eq} = \bar{\alpha}(l^{2/3} - 1)$ is not reliable here.

[4] Note that $\Delta\mu < 0$ in an undersaturated state.

with

$$G_l = -l\Delta\mu + G_l^{\rm eq} = -l\Delta\mu + \bar{\alpha}(l^{2/3} - 1). \tag{16}$$

The equilibrium number of clusters, $n_l^{\rm eq}$ or $\bar{n}_l$, is expressed in terms of the free energy G_l of the cluster. The ratio

$$S = \frac{n_1 - n_1^{\rm eq}}{n_1^{\rm eq}} = \frac{\delta n_1}{n_1^{\rm eq}}, \tag{17}$$

where $\delta n_1 = n_1 - n_1^{\rm eq}$, may be called a monomer supersaturation while the true supersaturation is defined as $(N - N^{\rm eq})/N^{\rm eq}$, where the total number density of atoms in the system is given by (5).

If the monomer density is increased to a value n_1 larger than $n_1^{\rm eq}$ at the same temperature, the evaporation rate is the same, but the impingement increases as shown in Fig.1(b). For large clusters, if they exist, the impingement rate exceeds the decay rate and the size increases. A particular size $l_{\rm c}$ of clusters, with which the two rates coincide, $n_1\sigma_{l_{\rm c}} = \lambda_{l_{\rm c}}$, or [5]

$$l_{\rm c}^{1/3} = \frac{2\bar{\alpha}}{3}\frac{1}{\ln(n_1/n_1^{\rm eq})} \approx \frac{2\bar{\alpha}}{3}\frac{n_1^{\rm eq}}{\delta n_1}. \tag{18}$$

This is the **critical cluster size**, which coincides with the thermodynamic definition. It is the size at which the free energy takes the minimum value[6]

$$\left.\frac{\partial G_l}{\partial l}\right|_{l_{\rm c}} = 0. \tag{19}$$

A cluster larger than $l_{\rm c}$ tends to grow, and a cluster smaller than $l_{\rm c}$ tends to shrink. The condition $j_l = 0$ determines an imaginary equilibrium state given by (13) or (15), $\bar{n}_l$, which is shown as the shaded area in Fig.1(b). The total number of atoms as well as the number of large clusters in this distribution $\bar{n}_l$ diverges.

If monomers are supplied to an equilibrium system (undersaturated or saturated), what happens is the following: the initial size distribution is something like that of Fig.1(a) and the clusters slowly grow as a result of collisions with monomers. When a cluster larger than $l_{\rm c}$ appears by chance, this cluster has a good chance to grow since $n_1\sigma_l > \lambda_l$ for $l > l_{\rm c}$. This is nucleation of a critical cluster for growth, and the cluster is called a **critical nucleus**. The first our problem is to describe the process of nucleation.

STEADY STATE NUCLEATION

Practical problems for nucleation theory are to estimate the time for a first nucleus to appear, and to determine the frequency of appearance of the critical nuclei. Time evolution of the system, when the monomer number (supersaturation) is changed, is difficult to study analytically, and we first study a steady state problem.

Steady State Distribution and Nucleation Rate

We consider the monomer density as a given constant n_1, and the numbers of very large clusters vanish. This is a reasonable approximation in an early stage in which all clusters are small and the total mass of the clusters larger than $l_{\rm c}$ is negligible compared to the monomer mass: $\sum_{l>l_{\rm c}}^{\infty} ln_l \ll n_1$. Theoretically, this state can be realized by eliminating very large clusters from the system and supplying monomers continuously to the system. As a result, there is stedy current $j_l^{\rm ss}$ in the cluster size space for $l \le l_{\rm max}$, where $l_{\rm max}$ is a cutoff size. The **steady state distribution** $n_l^{\rm ss}$ is determined by

$$j_l^{\rm ss} = \sigma_l n_1^{\rm ss} n_l^{\rm ss} - \lambda_{l+1} n_{l+1}^{\rm ss} = \text{constant} = j^{\rm ss} \tag{20}$$

---

[5] The critical size $l_{\rm c}$ is usually a large number, and, if necessary, we neglect the difference between l and $l+1$ for simplicity's sake.

[6] If one takes more general configurations into account than the spherical cluster, the critical point $l = l_{\rm c}$ is a saddle point: the free energy increases for any change of the cluster shape.

with the boundary condition, $n_1 = n_1^{\rm ss}$ and[7] $n_\infty = 0$. From (12), the decay coefficient in (20) can be expressed in terms of the imaginary equilibrium distribution as $\lambda_{l+1} = \sigma_l n_1 \bar{n}_l / \bar{n}_{l+1}$. By substituting this form into (20), we obtain a useful relation between the imaginary equilibrium distribution $\bar{n}_l$, which we already know in terms of the rate coefficients, and the steady state distribution $n_l^{\rm ss}$, which we want to know, as

$$\frac{n_l^{\rm ss}}{\bar{n}_l} - \frac{n_{l+1}^{\rm ss}}{\bar{n}_{l+1}} = \frac{j^{\rm ss}}{n_1 \sigma_l \bar{n}_l}. \tag{21}$$

Summing up (21) for l, and using $n_1^{\rm ss} = \bar{n}_1 = n_1$, we obtain

$$1 - \frac{n_l^{\rm ss}}{\bar{n}_l} = \sum_{l'=1}^{l-1} \frac{j^{\rm ss}}{n_1 \sigma_{l'} \bar{n}_{l'}}. \tag{22}$$

With the use of this relation we can calculate the steady nucleation rate and the steady state distribution.

With the boundary condition for $l \to \infty$, $n_l^{\rm ss}/\bar{n}_l = 0$, the steady state current, *i.e.* the **steady state nucleation rate**, $j_l^{\rm ss}$, is given by

$$\frac{1}{j_l^{\rm ss}} = \sum_{l'=1}^{\infty} \frac{1}{n_1 \sigma_{l'} \bar{n}_{l'}}. \tag{23}$$

The steady state distribution is also expressed in terms of the imaginary equilibrium distribution as

$$n_l^{\rm ss} = \bar{n}_l \left(1 - \frac{\displaystyle\sum_{l'=1}^{l-1} (\sigma_{l'} \bar{n}_{l'})^{-1}}{\displaystyle\sum_{l'=1}^{\infty} (\sigma_{l'} \bar{n}_{l'})^{-1}} \right). \tag{24}$$

In order to evaluate the steady state nucleation rate, we regard the discrete number l as a continuous variable

$$\frac{1}{j_l^{\rm ss}} = \int_1^{\infty} \frac{1}{n_1 \sigma_{l'} \bar{n}_{l'}} dl'. \tag{25}$$

Since $\bar{n}_{l'}$ changes exponentially fast, the integral can be evaluated by the saddle point integration at $l_{\rm c}$, where $\bar{n}_l = n_1 e^{-G_l/k_{\rm B}T}$ takes the minimum value. The result is

$$j^{\rm ss} \approx n_1 \sigma_{l_{\rm c}} \sqrt{-\frac{G''_{l_{\rm c}}}{2\pi k_{\rm B} T}}\, n_1 e^{-G_{l_{\rm c}}/k_{\rm B}T}. \tag{26}$$

It is the growth rate $n_1 \sigma_l \bar{n}_l$ at $l = l_{\rm c}$ multiplied by a factor from the Gaussian integral $\sqrt{-G''_{l_{\rm c}}/2\pi k_{\rm B} T}$, which is called the Zeldovich factor[10].

Approach to Steady State

Time Lag of Nucleation

If the monomer number is increased abruptly to a supersaturated value, we have to wait some period of time until a first critical nucleus appears. And nucleation becomes steady soon. The waiting time is called **time lag of nucleation**. In Fig.2, we show a numerical example of the change of the number of clusters larger than the critical size. This is the total number of nucleation events and nothing but the time integral of the current passing through the critical size,

[7] The steady distribution $n_l^{\rm ss}$ for large l is decreasing steeply because the larger a cluster, the faster it grows. And we may use this boundary condition.

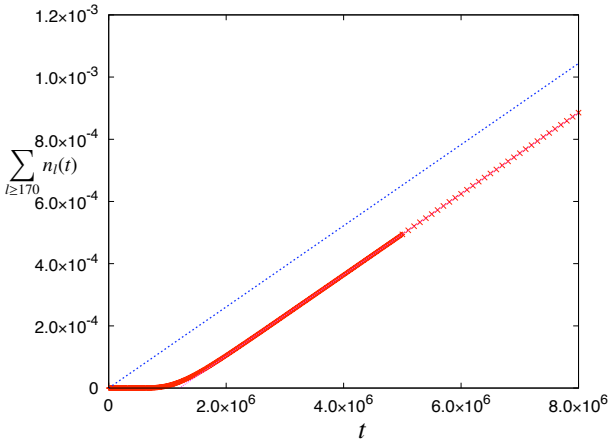

FIGURE 2. Number of supercritical nuclei for $S^{\rm ss} = 1.20$ ($S(0) = 4$). The red and green crosses are the numerical data, the dotted line (blue) represents the theoretical steady state rate $1.30 \times 10^{-10} t$ and the thin line (pink) the best linear fit: $1.30 \times 10^{-10}(t - 1.2 \times 10^6)$. (From [8])

$\int_0^t j_{l_c} dt$. In the numerical calculation, the initial distribution is assumed to be only monomers, and the equilibrium number is set constant $n_1^{\rm eq} = 10^{23}$. Other parameter values are fixed as[8] $\bar{\alpha} = 10$ and $a = 2 \times 10^{-28}$. Note that the time scale of change is basically determined by the product of the two factors: $n_1^{\rm eq} a$. The figure shows a linear increase after a time lag τ, which implies that nucleation becomes steady after the time lag. The time lag may be defined from the condition $j^{\rm ss}(t-\tau) = \int_0^t j_{l_c} dt$ for large t as

$$\tau = \int_0^\infty \left(1 - \frac{j_{l_c}(t)}{j^{\rm ss}}\right) dt, \tag{27}$$

where $j^{\rm ss}$ is current in the steady state. Theoretical estimation of the time lag gives the form[1, 11, 12]

$$\tau = s \frac{k_{\rm B} T}{n_1 \sigma_{l_c} |G''_{l_c}|}, \tag{28}$$

with s a numerical factor (~ 1, weakly increasing with the critical cluster size l_c).

The change of the distribution relative to the imaginary equilibrium distribution, $n_l(t)/\bar{n}_1$, up to an early stage of the steady state is shown in Fig3. During this period the distribution function expresses as $n_l(t)/\bar{n}_l$ expands to large clusters and approaches the steady state one with a well defined front[13]. The shape reaches the steady one $n_l^{\rm ss}/\bar{n}_l$ within a few times of τ in the figure. In this calculation the initial monomer supersaturation is $S(0) = 4.0$ ($n_1(0) = 5 \times 10^{23}$) but the monomers soon form small clusters and the monomer supersaturation drops to a steady value of $S^{\rm ss} = 1.20$ ($n_1(0) = 2.2 \times 10^{23}$) and remains this value for a long time. The value $S = 1.20$ corresponds to the supersaturation in the steady state and that in a real system. The critical nucleus size with $S^{\rm ss} = 1.20$ is $l_c = 170$, which has been used in Fig.2. The steady nucleation rate $j^{\rm ss} = 1.30 \times 10^{-10}$ obtained from the slope agrees well with the exact theoretical value

$$j^{\rm ss} = \left[\sum_{l=1}^{\infty} (n_1 \sigma_l \bar{n}_l)^{-1}\right]^{-1} = 1.30 \times 10^{-10}. \tag{29}$$

The saddle point evaluation (26) also gives a very good estimation: $j^{\rm ss} = 1.22 \times 10^{-10}$. The time lag here $\tau = 1.2 \times 10^6$ corresponds to[9] $s = 0.74$.

---

[8] The present choice of the parameters are rather arbitrary.

[9] The value s is smaller than other numerical results in the literature, possibly because we use the expression (11) instead of (10).

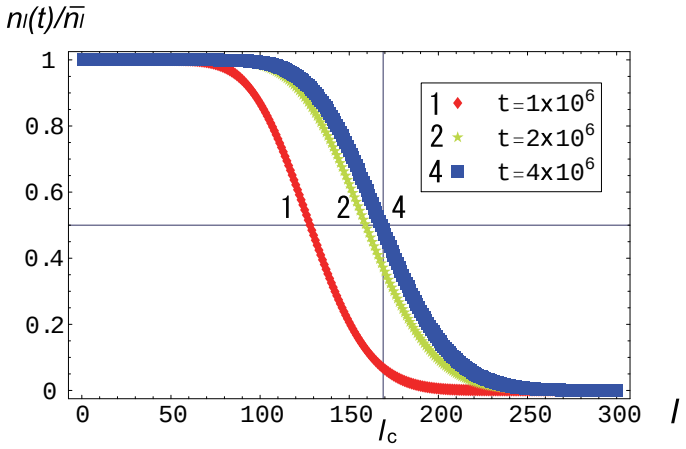

FIGURE 3. Scaled cluster distribution $n_l(t)/\bar{n}_l$ approaching the steady state one $n_l^{ss}/\bar{n}_l$ for $S^{ss} = 1.20$ ($S(0) = 4.0$). The cross lines indicate the critical nucleus l_c in n_l^{ss}. (From [8])

Continuum Variable and Fokker-Planck Equation

As we have done in (25), the discrete number l may be treated as a continuous variable. If the monomer number is kept constant, the current at a time may be written as

$$j_l(t) = n_1 \sigma_l \bar{n}_l \left(\frac{n_l(t)}{\bar{n}_l} - \frac{n_{l+1}(t)}{\bar{n}_{l+1}} \right) \Rightarrow -n_1 \sigma_l \bar{n}_l \frac{\partial}{\partial l} \frac{n_l(t)}{\bar{n}_l}. \tag{30}$$

Then the change of distribution is given by[10, 14]

$$\frac{\partial n_l(t)}{\partial t} = \frac{\partial}{\partial l} \left(n_1 \sigma_l \bar{n}_l \frac{\partial}{\partial l} \frac{n_l(t)}{\bar{n}_l} \right). \tag{31}$$

If we use the explicit form of the imaginary equilibrium distribution $\bar{n}_l = n_1 \exp(-G_l/k_B T)$, we obtain

$$\frac{\partial n_l(t)}{\partial t} = -\frac{\partial}{\partial l} \left(n_1 \sigma_l \frac{G_l'}{k_B T} n_l(t) \right) + \frac{\partial}{\partial l} \left(n_1 \sigma_l \frac{\partial n_l(t)}{\partial l} \right). \tag{32}$$

This is a form of the Fokker-Planck equation. The first term represents a drift effect towards a size of lower free energy, and the second term represents a diffusion effect in the size space, which tends to spread the distribution.

Starting from the distribution of an undersaturated equilibrium state (the shaded area of Fig.(a)), the diffusion, due to collision and evaporation, spreads the distribution, and its tail climbs the free energy hill against the drift. After the time lag, the tail of the distribution goes over the hill top (a saddle point in a configuration space) and leaks through the pass. The length of waiting time and the leaking rate are determined by the critical region of the free energy[15] and expressed in terms of l_c, G_{l_c} and G_{l_c}'' as (26) and (28).

EVOLUTION FROM NUCLEATION TO RIPENING

Variable Monomer Number

In a closed system the monomer number decreases during crystallization, and the condition $n_1(t) = n_1^{ss}$ should be removed. Rewriting the current as

$$j_l(t) = \sigma_l \left(n_1(t) - \frac{\lambda_l}{\sigma_l} \right) n_l(t) - (\lambda_{l+1} n_{l+1}(t) - \lambda_l n_l(t)), \tag{33}$$

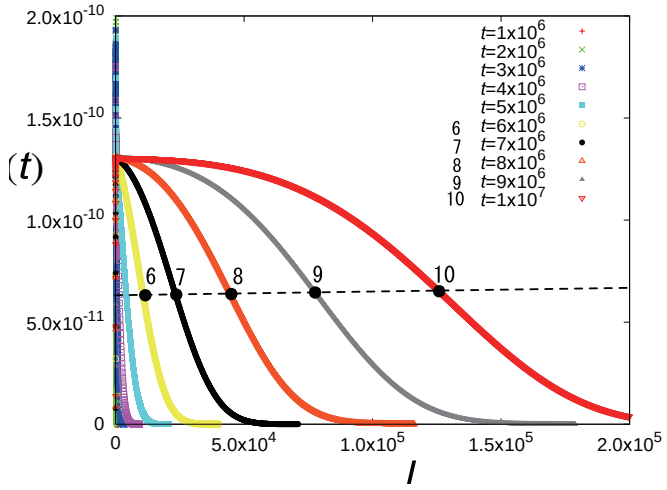

FIGURE 4. Current distribution $j_l(t)$ with $S^{\rm ss} = 1.20$ ($S(0) = 4.0$). The dashed line is $j_l = j^{\rm ss}/2$. The front cluster $l_{\rm f}(t)$ is indicated by the black dot in each distribution. (From [8].)

we can write the change of cluster numbers as[16]

$$\frac{\partial n_l(t)}{\partial t} = -\frac{\partial}{\partial l}\left(v_l(t)n_l(t)\right) + \frac{\partial^2}{\partial l^2}\left(\lambda_l n_l(t)\right), \tag{34}$$

where $v_l(t)$ is the drift velocity in the size space determined by $n_1(t)$ as

$$v_l(t) = \sigma_l\left(n_1(t) - \frac{\lambda_l}{\sigma_l}\right). \tag{35}$$

For our rate coefficient (11), the drift velocity is

$$\begin{aligned} v_l(t) &= \sigma_l\left[n_1(t) - n_1^{\rm eq}\left(1 + \frac{2\bar{\alpha}}{3}\frac{1}{l^{1/3}}\right)\right] &(36)\\ &= al^{2/3}\left(\delta n_1(t) - \frac{2\bar{\alpha}}{3}\frac{n_1^{\rm eq}}{l^{1/3}}\right) &(37)\\ &= Al^{2/3}\left(\frac{1}{l_{\rm c}^{1/3}(t)} - \frac{1}{l^{1/3}}\right), &(38)\end{aligned}$$

where $l_{\rm c}(t)$ is the temporary critical size determined by $\delta n_1(t)$ and the coefficient is

$$A = \frac{3a}{2\bar{\alpha}n_1^{\rm eq}}. \tag{39}$$

Change during the Steady State

After the time lag τ, the system can be considered as that in a steady state: we call this period a **stedy nucleation stage**. We plot in Fig.4 the current distribution $j_l(t)$, which is the number of monomers consumed for growth of the clusters at size l, obtained in the numerical calculation with the same parameters as in Fig3. The current $j_l(t)$ is a good measure to see the approach to the steady state: $j_l(t) = j^{\rm ss}$. Numerically, the position of the front $l_{\rm f}(t)$ defined by the mid value of the current, $j_{l_{\rm f}(t)}(t) = j^{\rm ss}/2$, obeys the deterministic equation (38), as expected. The distribution is not too far from the steady state one for $l \lesssim l_{\rm f}(t)$. The total number of monomer consumption for growth may be estimated

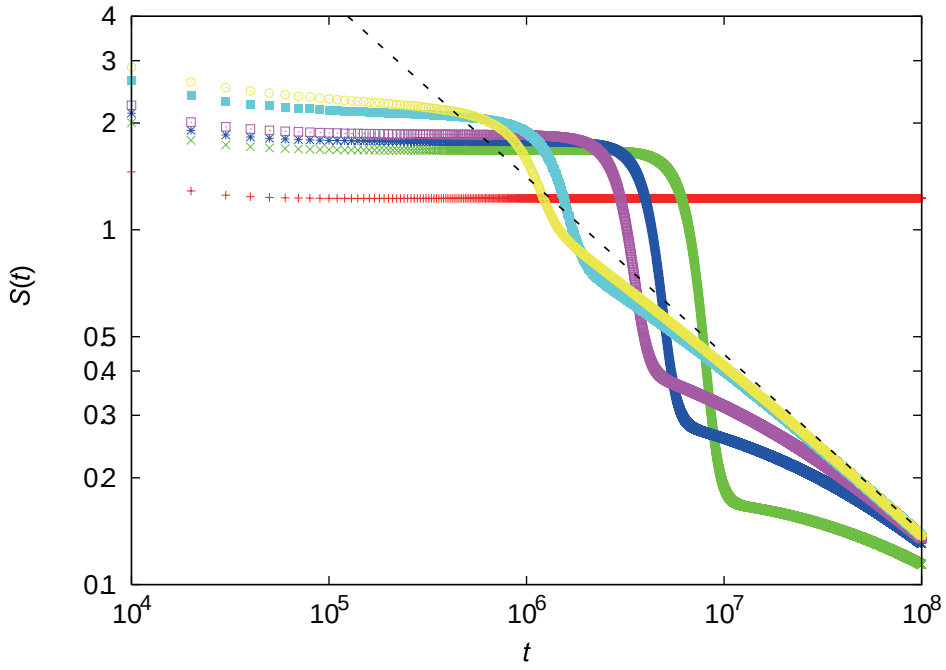

FIGURE 5. Change of supersaturation for various values of the initial monomer supersaturation; ∘(yellow): $S(0) = 19$, filled □(cyan): $S(0) = 14$, □(pink): $S(0) = 9$, ∗(blue): $S(0) = 8$, ×(green): $S(0) = 7$, +(red): $S(0) = 4$. The broken line is $S = 1.41 \times 10^3 t^{-1/2}$. (From [8].)

as

$$\dot{n}_1(t) = -\int_1^\infty j_l(t)dl \approx -j^{ss} l_f(t). \tag{40}$$

Although the monomer number is decreasing at the rate (40), no marked change in the supersaturation $S(t)$ occurs within the calculated time range since j^{ss} is very small for the supersaturation value $S^{ss} = 1.2$ ($S(0) = 4$).

According to (38) the front cluster size $l_f(t)$ first increases slowly because of the Gibbs-Thomson effect when $l_f(t) \sim l_c^{ss}$. Once the size becomes large ($l_f(t) \gg l_c^{ss}$), it increases rapidly and the second term is negligible. Thus

$$l_f(t) \approx \frac{A^3}{27 l_c^{ss}}(t - t_1)^3, \tag{41}$$

where $t_1 \sim \tau$ is a constant representing the nucleation time lag and a slow initial growth of $l_f(t)$. Then, from (40), the decrease in the monomer number is proportional to the fourth power of the duration:

$$\delta n_1^{ss} - \delta n_1(t) \sim \frac{j^{ss} A^3}{108 l_c^{ss}}(t - t_1)^4 = \frac{1}{108} j^{ss} (a \delta n_1^{ss})^3 (t - t_1)^4. \tag{42}$$

This equation characterizes the initial decrease in δn_1 from the steady state value.

End of the Steady Nucleation Stage

After the steady nucleation stage, the monomer consumption (42) becomes appreciable so that the value of j_l, which is proportional to δn_1, the growth rate of the distribution front l_f, and the size of critical nucleus l_c change. Accurate evaluation of these changes needs detailed information of the size distribution, and numerical calculation is necessary. In Fig.5 we show the change of relative supersaturation $S(t)$ in a logarithmic scale for various initial values of $n_1(0)$.

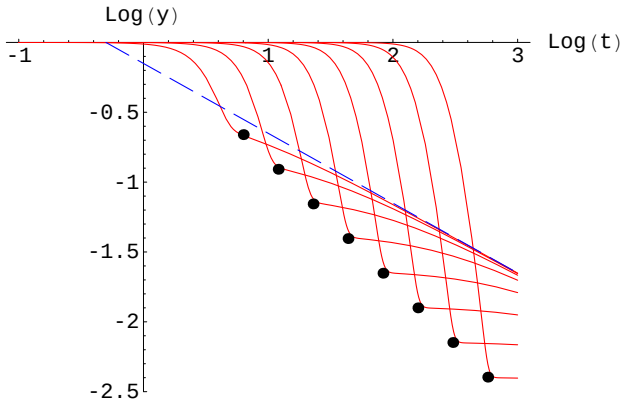

FIGURE 6. The scaled monomer numbers, $y = \delta n_1(t)/\delta n_1^{\rm ss}$, derived from the solution of (47) for $c = 10^{-2}, 10^{-3}, \cdots, 10^{-9}$ (left to right). The straight line is the asymptotic form, and the black dots are the transition points to the late stage. (From [8].)

With relatively "weak" supersaturation as $S(0) = 4$ (the steady state value: $S^{\rm ss} = 1.20$), the decrease of S is not appreciable within the calculated time. With a stronger supersaturation as $S(0) = 7$ ($S^{\rm ss} = 1.7$), the supersaturation drops down to $S \approx 0.17$ in a rather short period and then decreases much more slowly. This sharp drop of supersaturation is due to free growth of nucleated clusters. The monomer consumption is accelerated because the supercritical clusters nucleated in an early stage have become large. The monomer consumption ends because supersaturation has dropped and small clusters nucleated later start to dissolve. With a stronger initial supersaturation, the supersaturation behaves similarly but with a shorter steady nucleation stage and a smaller drop of S, in agreement with experiment[17].

Simplified Qualitative Description of Supersaturation

To understand qualitatively the change of supersaturation as time, the following simplified model with a single variable may be useful. We replace (40) by

$$\frac{dn_1(t)}{dt} = -j^{\rm ss}\frac{\delta n_1(t)}{\delta n_1^{\rm ss}}\left(l_{\rm f}(t) - l_{\rm c}(t)\right), \tag{43}$$

where we have assumed that the monomer consumption is proportional to the temporary supersaturation (or the excess monomer number), $\delta n_1(t)$, and that the range of growing clusters is from the critical size $l_{\rm c}(t)$ to the front cluster size $l_{\rm f}(t)$. The latter, neglecting the Gibbs Thomson effect, changes as

$$l_{\rm f}^{1/3}(t) = (l_{\rm c}^{\rm ss})^{1/3} + \frac{a}{3}\int_{t_1}^{t}\delta n_1(t')dt' \tag{44}$$

from (37), and the temporary critical size is

$$l_{\rm c}(t) = l_{\rm c}^{\rm ss}\left(\frac{\delta n_1^{\rm ss}}{\delta n_1(t)}\right)^3, \tag{45}$$

from (18). The detailed change of the form of distribution is completely neglected. All quantities are expressed in relation to their values at the steady nucleation stage.

With the use of a new variable

$$z(t) = \frac{1}{b} + \frac{1}{\delta n_1^{\rm ss}}\int_0^t \delta n_1 dt', \tag{46}$$

the time evolution equations can be cast into the single equation as

$$\frac{d^2z(t)}{dt^2} = -c\frac{dz(t)}{dt}\left[(bz(t))^3 - \left(\frac{dz(t)}{dt}\right)^{-3}\right]. \tag{47}$$

The parameters are defined by

$$b = \frac{a\delta n_1^{\rm ss}}{3(l_{\rm c}^{\rm ss})^{1/3}} = \frac{a(\delta n_1^{\rm ss})^2}{2\bar{\alpha} n_1^{\rm eq}}, \qquad c = \frac{j^{\rm ss} l_{\rm c}^{\rm ss}}{\delta n_1^{\rm ss}}. \tag{48}$$

In (47), we have shifted the origin of time to $t = t_1$. The monomer number is given by

$$\delta n_1(t) = \delta n_1^{\rm ss} \dot{z}(t). \tag{49}$$

The initial conditions are $\dot{z}(0) = 1$ and $z(0) = 1/b$. Numerical integration of (47) is easy and the solutions for various values of c are shown in Fig.6.

With the change of the initial supersaturation $S(0)$, the steady nucleation rate $j_{\rm ss}$ changes markedly, and $j_{\rm ss}$ controls the initiation of the sharp drop of supersaturation. The equation (47) does not include the time lag τ and t_1, and the drop of S in Fig.6 occurs too early, but the transition point from the free growth stage to the ripening stage is reproduced qualitatively well[10].

Ostwald Ripening

As seen in Fig.6, all the solutions approach, after a slow change of S, an asymptotic line, which is obtained from the condition that the quantity in the square bracket of (47) vanishes: $\delta n_1(t) = \left(\bar{\alpha} n_1^{\rm eq}/at\right)^{1/2}$. The data of direct numerical calculation (Fig.5) also indicate a similar asymptotic behavior. The stage of slow change is the **Ostwald ripening stage**. Here the drop of supersaturation is compensated by melting of clusters smaller than the critical size $l_{\rm c}(t)$, which has increased with consumption of monomers by the growth of large clusters.

The asymptotic behavior of $S(t)$ in the Ostwald ripening is well described by the **Lifshitz-Slyozov-Wagner(LSW) theory**[5, 6], which is a mean field description of the system. Since fluctuation is less important for large clusters, the LSW theory uses (34) without the diffusive second term:

$$\frac{\partial n_l(t)}{\partial t} + \frac{\partial}{\partial l}\left(v_l(t) n_l(t)\right) = 0, \tag{50}$$

with the change of cluster size

$$\frac{dl^{1/3}(t)}{dt} = \frac{A}{3}\left(\frac{1}{l_{\rm c}^{1/3}(t)} - \frac{1}{l^{1/3}(t)}\right), \tag{51}$$

from (38). In the ripening stage small clusters are melting while large clusters are growing. The divide is the critical cluster size $l_{\rm c}(t)$, which increases as the supersaturation decreases. The cluster size distribution is shifting to large clusters, and the total number of clusters is decreasing. Let us assume that the shape of this distribution does not change in time and only the characteristic size changes. This size must be the critical size $l_{\rm c}(t)$. Thus the distribution has the scaling form $n_l(\tilde{t}) \sim \nu(\lambda)$ with $\lambda = l/l_{\rm c}(\tilde{t})$, where $\tilde{t}$ is the time measured from an arbitrary starting time in the ripening stage with a proper unit. Since the number of atoms in the clusters are roughly the total number[11], the distribution has the form

$$n_l(\tilde{t}) = \frac{l_{\rm c}(0)}{l_{\rm c}^2(\tilde{t})}\nu(\lambda), \tag{52}$$

which should satisfy the number conservation

$$\int_0^\infty l n_l(\tilde{t}) dl = l_{\rm c}(0) \int_0^\infty \lambda\, \nu(\lambda) d\lambda = N. \tag{53}$$

---

[10] The location of the transition points seems to obey a power law as indicated by black dots in Fig.6

[11] Contrary to the initial nucleation stage, the monomer number in the late stage is negligible compared to the number of atoms in all other clusters.

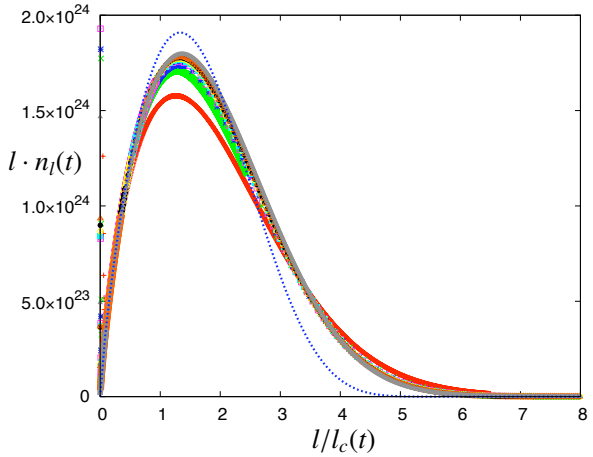

FIGURE 7. Change of the mass distribution $ln_l(t)$ with an extremely high supersaturation $S(0) = 49.0$. The dotted line (blue) is the LSW scaling solution $n_l^{\rm LSW}$, and the marks are the data from $t = 10^6$ (red, bottom) to $t = 2 \times 10^7$ (grey, top). (From [8].)

The form of the scaling function is[8]

$$\nu(\lambda) = \frac{8e^3}{\lambda^{1/3}(2-\lambda^{1/3})^5} e^{-6/(2-\lambda^{1/3})} \nu_0 \tag{54}$$

with the constant[12] $\nu_0 = 1.04529(N/l_{\rm c}(0))$, and the range of λ is limited to $0 < \lambda < 8$. The total number of clusters at time $\tilde{t}$ is

$$N_{\rm cluster}(\tilde{t}) = \int_0^\infty n_l(\tilde{t}) dl = \frac{l_c(0)}{l_c(\tilde{t})} \int_0^8 \nu(\lambda) d\lambda = 1.04529 \frac{N}{l_c(\tilde{t})}. \tag{55}$$

The asymptotic form of the critical size is given by

$$l_{\rm c}^{1/3}(t) = \frac{1}{3}\sqrt{a\bar{\alpha} n_1^{\rm eq} t}, \tag{56}$$

and therefore the supersaturation changes as[8]

$$\delta n_1(t) = 2\sqrt{\frac{\bar{\alpha} n_1^{\rm eq}}{a}} t^{-1/2}. \tag{57}$$

In Fig.5 the LSW form (57), $S = \delta n_1(t)/n_1^{\rm eq} = 1.41 \times 10^3 t^{-1/2}$, is indicated by the broken line, which all the data seem to approach. (The result of the simplified model fails by a factor two.) Mass distribution $ln_l(t)$ obtained with a very high initial value[13] $S(0) = 49.0$ along with the LSW scaling solution $ln_l^{\rm LSW}$ is shown in Fig.7. Although the shape is somewhat similar, its approach to the exact asymptotic form $n_l^{\rm LSW}$ is known to be extremely slow[18].

The final power law decrease of supersaturation (57) or the increase of critical size (56) depends on the form of σ_l. So far we have assumed the kinetics-limited growth (the rate is proportional to the surface area) $\sigma_l = al^{2/3}$. If growth is limited by a bulk diffusion process, the rate is proportional to the surface area devided by the diffusion length and $\sigma_l \sim l^{1/3}$, then we have $\delta n_1(t) \sim l_{\rm c}^{-1/3}(t) \sim t^{-1/3}$. This is the well-known coarsening law for diffusion growth confirmed by many experiments.

---

[12] The normalization is $\nu_0^{-1} \int \nu(\lambda) d\lambda = 1$, and $\nu_0^{-1} \int \lambda \nu(\lambda) d\lambda = 0.956676 = 1/1.04529$.

[13] With smaller initial supersaturation the late stage cannot be reached within our calculation time.

Is the Classical Nucleation Theory Reliable?

We have studied the behavior of the CNM from the beginning to the end. Obviously, the final state in reality is a big single crystal in the whole system, but not the continuous distribution of the CMN, which is an artifact due to the continuous treatment of the model. We should not forget that CNM is a rate equation treatment of a probabilistic model. The CNM assumes the spherical shape of the clusters and neglects all correlations[4]. Despite these limitations, the CNM model seems to describe the nucleation process rather well[11]. The predicted nucleation rate, however, sometimes differs orders of magnitude from the experimental data, and reconsideration of the CNT is necessary. Recent advancement of the computer and the statistical mechanical treatment[19] make direct molecular dynamics simulation of nucleation possible. For example, a recent study of crystal nucleation of an undercooled Lennard-Jones liquid shows, about the nucleation pathways, that critical clusters can be small and compact, with a high degree of stable fcc ordering, but also loose and more metastable bcc ordered[20].

What is really happening during nucleation is rather difficult to observe in real bulk systems. On crystal surfaces, there are more opportunities for observation of atomic clusters, and many detailed studies have been attempted[21].

CHIRALITY CONVERSION OF CRYSTALS BY GRINDING

The CNM has been applied to many systems with considerable success. In this section We will present one recent application of a generalized version of this model. The problem is related to competing crystallization of two chiral pair of crystals.

Chiral Symmetry Breaking and Chirality Conversion in Crystallization

Striking chirality conversion of $NaClO_3$ crystals by grinding in a saturated solution was discovered by Viedma[22]. A molecule of $NaClO_3$ is achiral, but its crystal takes right (R) and left (L) types of structures[14]. The material is known to show spontaneous chiral symmetry breaking during nucleation growth with stirring[23]. When the solution is highly supersaturated, both types of crystals nucleate, and, without stirring, we will obtain about the same amount of R and L crystals, that is, the system is *racemic*. If the solution is stirred, however, almost all crystals obtained in a single run are either R or L crystals at even odds, and each system is *homochiral*. The cause of this phenomenon is attributed to secondary nucleation, by which the type of crystals that nucleated first become predominant[24, 25]. The newly discovered chirality conversion of the crystal structures occurs when both types coexist in a solution at first, and by grinding crystals, the minority type disappears. The transition from a racemic (mixed) state into a homochiral state is very puzzling since the two chiral states are energetically equal. Recently Noorduin et al. reported a similar phenomenon in an organic molecule system[26]. In the organic system, a molecule has chirality, which can change in a solution with an added base, and the chiral molecules form crystals of the respective chiralities. Therefore the conversion of crystal chirality implies the simultaneous conversion of molecular chirality: simple grinding converts the molecular chirality of the minority type. Recent review of experiment in organic systems is given in [27].

Reaction Model for the Chirality Conversion

Several models have been proposed to explain the chirality conversion[28, 29, 30, 31, 32, 33]. The first model proposed to explain this extraordinary phenomenon was a simple reaction type model that takes crystallization of clusters into account[28]. The important features of the model are enhanced formation of subcritical chiral clusters by grinding and incorporation of the clusters into crystals of the same chirality. This nonlinear process amplifies a small initial imbalance of chiral components, and the minor species is completely converted into the major species.

The model involves five mass variables(Fig.8(a)): two kinds of chiral crystals (X and Y), whose masses are denoted by x and y, two kinds of chiral clusters (X_u and Y_u), denoted by x_u and y_u, and achiral monomers (Z), denoted by

[14] The two chiral pairs are called dextrorotatory (D) and levorotatory (L), or rectus (R) and sinister (S) in different contexts. In this paper, we simply use the words, right and left.

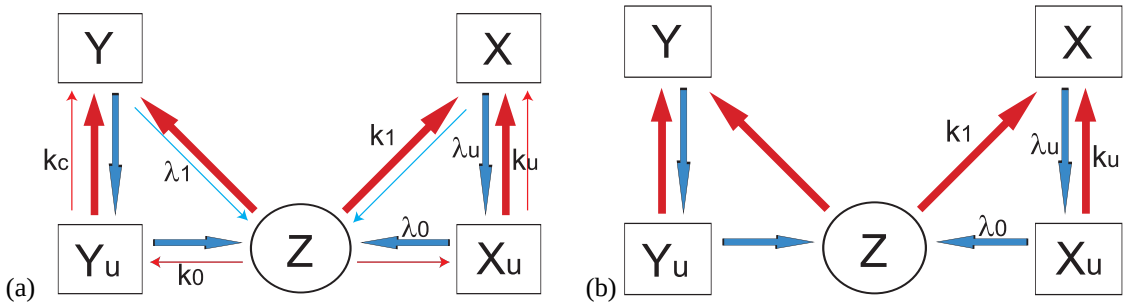

FIGURE 8. (a) Original reaction-type model[28]. X and Y: chiral crystals, X_u and Y_u: subcritical chiral clusters, and Z: achiral molecules. (b) Minimal model for chirality conversion[35]. (From [31].)

z. Since the system is always ground, the size distribution of crystals and the concentration in the solution must be steady, and we may describe the system with masses of the five components. The following reactions are assumed:

1) formation of chiral clusters ($Z + Z \rightarrow X_u$ or $Z + Z \rightarrow Y_u$),
2) nucleation of chiral clusters ($X_u + X_u \rightarrow X$ and $Y_u + Y_u \rightarrow Y$),
3) growth of crystals by incorporating achiral monomers ($X + Z \rightarrow X$ and $Y + Z \rightarrow Y$),
4) growth of crystals by incorporating chiral clusters ($X + X_u \rightarrow X$ and $Y + Y_u \rightarrow Y$),
5) decay of chiral clusters , ($X_u \rightarrow Z + Z$ and $Y_u \rightarrow Z + Z$),
6) dissolution of achiral monomers ($X \rightarrow X + Z$ and $Y \rightarrow Y + Z$),
7) dissolution of chiral clusters ($X \rightarrow X + X_u$ and $Y \rightarrow Y + Y_u$).

Fig.9 shows an example of numerical calculation starting with abundant monomers and a little excess of right chiral crystals X compared to Y. Within a short period ~ 5, the system seems to reach a steady state with almost the same amount of X and Y, and the system is racemic. In the long run, however, the racemic state is unstable and the tiny imbalance of X and Y is amplified exponentially. The final state is homochiral and contains little amount of the minor species Y[15]. The exponential amplification of enantiomeric excess (chirality imbalance) agrees with the experiment[22]. With a small amount of chiral crystals X in a supersaturated solution, the model also seems to reproduce the spontaneous symmetry breaking observed in a supersaturated solution[23].

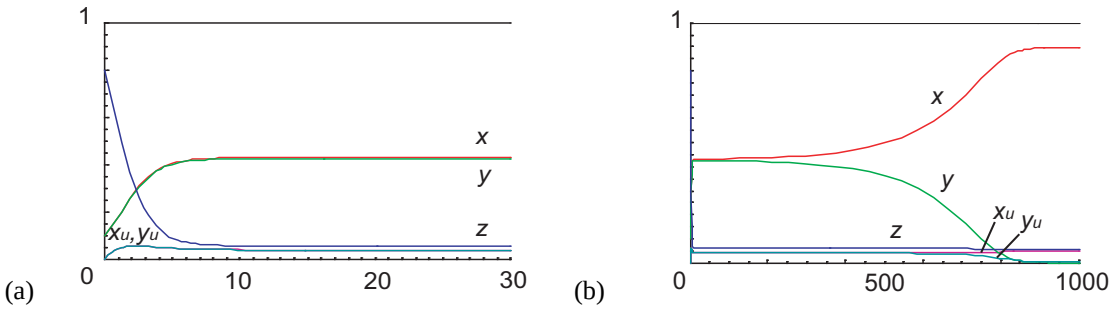

FIGURE 9. Time evolution for $x(0) = 0.101$, $y(0) = 0.100$ and $x_u(0) = y_u(0) = 0$. (From [28].)

[15] Since all the processes have their inverse reaction, complete distinction of Y does not occur.

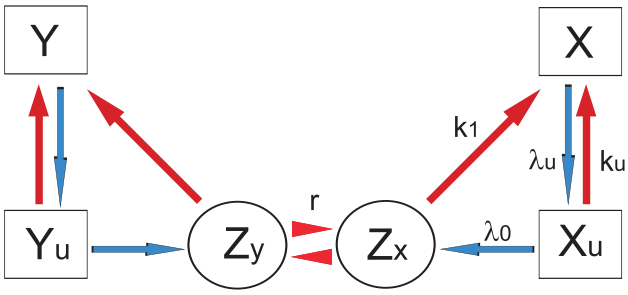

FIGURE 10. Reaction type model for organic systems. Monomers are chiral and transform each other in a solution. (From [31].)

McBride and Tully[35] showed that the model may be simplified for the chirality conversion problem. Since both types of crystals are present from the beginning, the nucleation process is not really necessary. Without the processes 1), 2) and 6), the system behaves essentially in the same way. The reaction type model is also applicable to the organic system, with replacement of the monomer component from achiral Z to equilibrating(racemizing) chiral pairs Z_x and Z_y (See Fig.10).

Although the simple reaction type models reproduce the experimental behavior qualitatively, validity of the assumptions behind them should be clarified. As an application of the CNM, we study size distribution of the chiral solid clusters for the chirality conversion problem.

Generalized Classical Nucleation Model with Grinding

The essential assumption of the reaction type models is that the relative size distribution of crystals does not change during grinding. To test the validity of this assumption, we generalize the CNM and performe numerical integration. Since the chiral crystallization problem involves two types of clusters, we need to distinguish the numbers of right-handed and left-handed clusters as n_l^{R} and n_l^{L} for $l \geq 2$. Here we assume, for simplicity, monomers are achiral and all clusters ($l \geq 2$) are chiral, although in the $NaClO_3$ case clusters larger than trimers are chiral[22]. The cluster reactions included in the generalized CNM are

$$\mathrm{A}+\mathrm{A} \;\leftrightarrow\; \mathrm{R}_2 \text{ or } \mathrm{L}_2, \tag{58}$$

$$\mathrm{A}+\mathrm{R}_l \leftrightarrow \mathrm{R}_{l+1} \qquad \mathrm{A}+\mathrm{L}_l \leftrightarrow \mathrm{L}_{l+1} \qquad \text{for } 2 \leq l \leq l_{\max}-1, \tag{59}$$

where A is the achiral molecule and R_l and L_l represent right and left types of clusters consisting of l molecules. The reactions in (58) and (59) are the usual CNM processes. The crucial point of the model is that incorporation of chiral dimers to clusters of the same chirality occurs:

$$\mathrm{R}_2+\mathrm{R}_l \leftrightarrow \mathrm{R}_{l+2} \qquad \mathrm{L}_2+\mathrm{L}_l \leftrightarrow \mathrm{L}_{l+2} \qquad \text{for } 2 \leq l \leq l_{\max}-2. \tag{60}$$

We have assigned a maximum cluster size $l_{\max}$ to model the grinding process. The largest clusters, $\mathrm{R}_{l_{\max}}$ and $\mathrm{L}_{l_{\max}}$, are assumed to decompose into small clusters at a given rate $\lambda^{\mathrm{gr}} n_{l_{\max}}^{\mathrm{R,L}}$. The dimer incorporation to the larger clusters occurs in the same way as the monomer incorporation at the rate $\sigma_l^{\mathrm{d}} n_2^{\mathrm{R,L}} n_l^{\mathrm{R,L}} = a^{\mathrm{d}} l^{2/3} n_2^{\mathrm{R,L}} n_l^{\mathrm{R,L}}$. The corresponding decay rate, $\lambda_l^{\mathrm{d}} n_l^{\mathrm{R,L}}$, satisfies the detailed balance condition. The two rate constants for dimers, $\sigma^{\mathrm{d}} = a^{\mathrm{d}} l^{2/3}$ and λ^{d}, are probably smaller than those for monomers, $\sigma = a l^{2/3}$ and λ.

Numerical Results

We first perform numerical integration of the generalized CNM without grinding, and find the usual OR, which may cause slow chirality conversion. Then we will include the grinding effect by limiting the maximum size of clusters and introducing new terms.

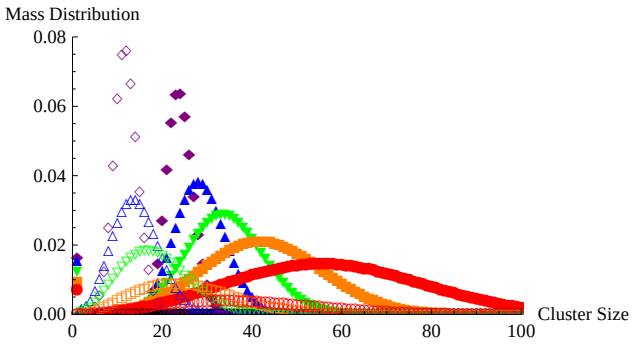

FIGURE 11. Evolution of the mass distribution during OR without grinding: $ln_l(t)$ at $t = 20$ (purple diamond), $t = 80$ (blue triangle), $t = 160$ (green inverted triangle), $t = 320$ (orange square), $t = 640$ (red circle). Filled marks are R and empty marks are L. The initial conditions are $n_{10}^{\mathrm{R}}(0) = 0.45/10$, $n_{20}^{\mathrm{R}}(0) = 0.4/20$, and $n_1(0) = 0.05$. The parameters are $n_1^{\mathrm{eq}} = 0.001$, $a = a^{\mathrm{d}} = 1.0$, $\lambda^{\mathrm{gr}} = 0$ and $l_{\max} \gg 100$.

Without Grinding

If crystals of one type is larger than those of the other, Ostwald ripening (OR) causes chirality conversion *without grinding*[36]. Figure 11 shows the mass distribution, $ln_l^{\mathrm{R,L}}$, without grinding ($\lambda^{\mathrm{gr}} = 0$ and $l_{\max} \to \infty$) under the initial condition with more small L crystals ($l = 10$) and fewer large R crystals($l = 20$). Other parameter values used are $n_1^{\mathrm{eq}} = 0.001$ and[16] $a = a^{\mathrm{d}} = 1.0$. The peak of L clusters gradually diminishes and that of R clusters grows. As time proceeds, the mass of R clusters will increase more and more at the cost of L clusters. The final state that OR brings about in reality is obviously a single R crystal. However, it takes too long time to realize the final state of a single crystal in a macroscopic system. The problem posed by the grinding experiments[22, 26] is that whether crystals of similar size distributions produced by grinding can realize the amplification of the initial chirality imbalance. It is important to realize the chirality conversion in a time scale independent of the system size[34]. To see the effect of grinding, we introduce the maximum cluster size and decomposition of these clusters to smaller clusters.

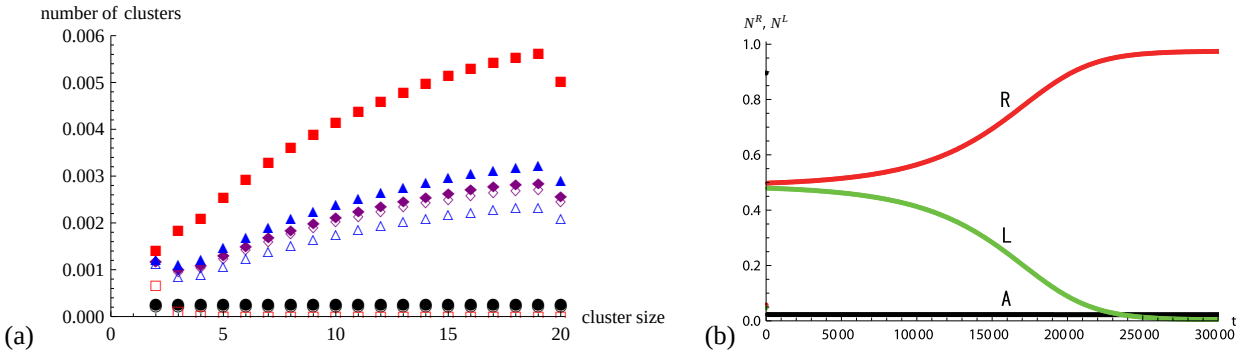

FIGURE 12. (a) Time evolution of the distribution function $n_l(t)$ at $t = 0$ (black circle), $t = 10^3$ (purple diamond), $t = 10^4$ (blue triangle), $t = 10^5$ (red square). Filled marks are R and empty marks are L. The parameters are $\lambda^{\mathrm{gr}} = 0.1$ and $l_{\max} = 20$. Other parameters are the same as those in Figs.11. (b) Number of molecules (normalized by the total number) as achiral monomers $n_1(t)$ (A, black) and in R and L clusters $N^{\mathrm{R}}(t)$ (R, red), $N^{\mathrm{L}}(t)$ (L, green).

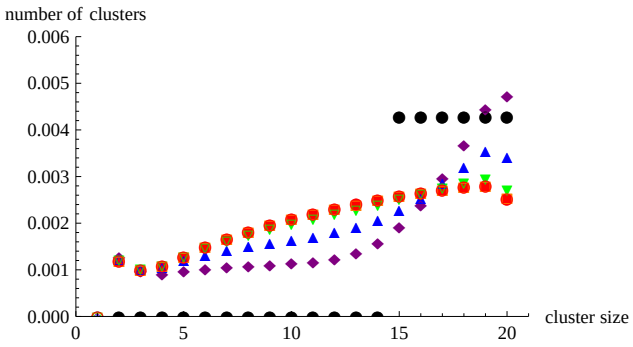

FIGURE 13. Time evolution of the distribution function $n_l(t)$ at $t = 0$ (black circle), $t = 20$ (purple diamond), $t = 40$ (blue triangle), $t = 80$ (green inverted triangle), $t = 160$ (orange square), $t = 10^4$ (red circle).

With Grinding

Fig. 12 shows time evolution of the size distribution and the number of atoms in each kind of chiral clusters[9]. The number of clusters is normalized by the total number of molecules, $N = n_1 + N^{\rm R} + N^{\rm L}$, where $N^{\rm R,L} = \sum_{l=2}^{l_{\rm max}} l n_l^{\rm R,L}$, so that the total number is unity. The parameter values used are: $n_1^{\rm eq} = 0.001$, $\lambda^{\rm gr} = 0.1$, $a = a^{\rm d} = 1.0$, and $l_{\rm max} = 20$. The initial distribution is set slightly R-rich: $n_l^{\rm R} = 0.11/l_{\rm max}^2$, $n_l^{\rm L} = 0.9/l_{\rm max}^2$ (circles in Fig. 12) and $n_1 = 1 - N^{\rm R} - N^{\rm L} (= 0.8955$; the initial solution is strongly supersaturated). At first the cluster numbers $n_l^{\rm R,L}$ increase rapidly and reach a "quasi-steady" (slowly-varying) distribution with a small chirality imbalance (diamonds in Fig. 12). After $t \approx 200$, the difference of $N^{\rm R}$ and $N^{\rm L}$ increases slowly and exponentially with an amplification rate $\omega = 2.14 \times 10^{-4}$. The exponential amplification of the chirality imbalance continues until $t \approx 1.7 \times 10^4$ when saturation sets in as shown in Fig. 12(b). This feature is similar to that observed in Fig. 9(b).

Although the size distributions of R and L clusters markedly change, their shape and the total distribution $n_l^{\rm R}(t) + n_l^{\rm L}(t)$ remain approximately the same during the amplification of chirality imbalance. The chirality conversion occurs without changing the total size distribution, in contrast to the chirality conversion by simple OR (Fig. 11). The Gibbs-Thomson effect, which causes the chirality conversion without grinding, is certainly working in the present system with grinding. However, additional factors, incorporation of chiral clusters and grinding, are necessary to accelerate growth of the majority species. If one of the two factors, cluster reaction and grinding, is lacking (*i.e.* $a^{\rm d} = 0$ or $\lambda^{\rm gr} = 0$), the exponential amplification of the initial chirality imbalance does not occur. If we start with a chiral-symmetric initial condition, $n_l^{\rm R}(0) = n_l^{\rm L}(0)$, very different from that of Fig. 12(a) (black circles in Fig. 13), the final state with grinding is symmetric as indicated by red circles in Fig. 13(a). The final distribution is very similar to the intermediate state at $t \approx 10^3$ in Fig. 12(a), which is a half of the total distribution $n_l^{\rm R}(t) + n_l^{\rm L}(t)$ after $t \approx 10^3$. This symmetric (racemic) state is unstable against a small asymmetric perturbation. If the initial condition is a slightly asymmetric distribution of somewhat arbitrary shape, the distribution first approaches the unstable racemic distribution quickly, and then the asymmetry is slowly amplified. The final state is that in Fig. 12 (or the state with R and L exchanged), which is unique and almost homochiral with few small minority clusters. Thus, the implicit assumptions of the reaction type models[28, 31] that grinding produces a steady cluster size distribution is justified. From the unstable racemic state to the final homochiral state, the number of monomers changes slightly [$n_1(10^3) = 0.02248$ and $n_1(10^5) = 0.02205$]. These numbers of monomers correspond to the critical cluster sizes $l_{\rm c} = 9.83$ and $l_{\rm c} = 10.01$, and OR apparently does not play the leading role.

CONCLUDING REMARKS

The classical nucleation model is simple and useful since it describes the entire process of crystal growth from a supersaturated environment: from the initial stage of nucleation through free growth of crystallites to the final stage of

[16] The result is very similar without dimer reaction, $a^{\rm d} = 0$.

Ostwald ripening. It provides us with consistent view of evolution of the system although to have quantitative view we need to add various processes to the model. It may be used for more general situations such as the chirality conversion with grinding crystals.

ACKNOWLEDGMENTS

The author thanks K. Koyama and H. Katsuno, who performed the studies of the CMN and the chirality conversion with me. He also acknowledges financial assistance from Japan Society for the Promotion of Scienece.

REFERENCES

1. D. Kashchiev, *Nucleation: Basic Theory with Applications* (Butterworth-Heinemann, 2000).
2. L. Farkas Z. Phys. Chem. **125**, 236 (1927).
3. R. Becker and W. Döring, Ann. Phys. **24**, 719 (1935).
4. The effects of correlations and collisions of clusters have been studied. See, for example: K. Binder and D. Stauffer, Adv. Phys. **25**, 342 (1976); M. Marder, Phys. Rev. A **36**, 858 (1987); C. Sagui and M. Grant, Phys. Rev. E **59**, 4175 (1999).
5. I. M. Lifshitz and V. V. Slyozov, J. Phys. Chem. Solids, **19**, 35 (1961).
6. C. Wagner, Z. Elektrochem. **65**, 581 (1961).
7. Various theories of first order phase transitons are described in: A. Onuki, *Phase Transition Dynamics*, (Cambridge University Press, Cambridge, 2002).
8. M. Uwaha and K. Koyama, J. Cryst. Growth, **312**, 1046-1054 (2010).
9. M. Uwaha and H. Katsuno, J. Phys. Soc. Jpn., **78**, 023601 (2009). All the numerical data of time t in this paper should be divided by 10, and, as a result, all the amplification rates should be multiplied by 10.
10. Ya. B. Zeldovich, Acta Physicochim. (USSR) **18**, 1 (1943).
11. K. F. Kelton, in *Solid State Physics*, ed. H. Ehrenreich and D. Turnbull (Academic, New York, 1991), Vol.45, pp.75-177.
12. D. T. Wu, in *Solid State Physics*, ed. H. Ehrenreich and F. Spaepen (Academic, New York, 1996), Vol.50, pp.37-187.
13. J. C. Neu, L. L. Bonilla, and A. Carpio, Phys. Rev. E **71**, 021601 (2005).
14. J. Frenkel, 'Kinetic Theory of Liquids', (Oxford University, Oxford, 1946).
15. D. Kashchiev, Surf. Sci. **14**, 209 (1969).
16. O. Penrose, J. Stat. Phys. **89**, 305 (1997).
17. J. Garside, C. Gaska, and J. W. Mullin, J. Cryst. Growth **13/14**, 510 (1972).
18. B. Meerson, L. M. Sander, and P. Smereka, Europhys. Lett. **72**, 604 (2005).
19. P. G. Bolhuis, D. Chandler, C. Dellago, and P. L. Geissler, Ann. Rev. Phys. Chem. **54**, 20 (2002).
20. D. Moroni1, P. R. ten Wolde, and P. G. Bolhuis, Phys. Rev. Lett. **94**, 235703 (2005).
21. For a recent review, see: J. W. Evans, P. A. Thiel, and M. C. Bartelt, Surf. Sci. Rep. **61**, 1 (2006).
22. C. Viedma, Phys. Rev. Lett. **94**, 065504 (2005).
23. D. K. Kondepudi, R. Kaufman, and N. Singh, Science **250**, 975 (1990).
24. R.-U. Qian and G. D. Botsaris, Chem. Eng. Sci. **53**, 1745 (1998).
25. For a review of related problems, D. K. Kondepudi, and K. Asakura, Acc. Chem. Res. **34**, 946 (2001).
26. W. L. Noorduin, T. Izumi, A. Millemaggi, M. Leeman, H. Meekes, W. J. P. Van Enckevort, R. M. Kellogg, B. Kaptein, E. Vlieg, and D. G. Blackmond, J. Am. Chem. Soc. **130**, 1158 (2008).
27. W. L. Noorduin, E. Vlieg, R. M. Kellogg, and B. Kaptein, Angew. Chem. Int. Ed. **48**, 9600 (2009).
28. M. Uwaha: J. Phys. Soc. Jpn. **73**, 2601 (2004).
29. J. H. E. Cartwright, O. Piro, and I. Tuval, Phys. Rev. Lett. **98**, 165501 (2007).
30. W. L. Noorduin, H. Meekes, W. J. P. van Enckevort, A. Millemaggi, M. Leeman, B. Kaptein, R. M. Kellogg, and E. Vlieg, Angew. Chem. **120**, 6545 (2008).
31. M. Uwaha, J. Phys. Soc. Jpn. **77**, 083802 (2008).
32. Y. Saito and H. Hyuga, J. Phys. Soc. Jpn **77**, 113001 (2008).
33. Y. Saito and H. Hyuga, J. Phys. Soc. Jpn **78**, 104001 (2009).
34. H. Katsuno and M. Uwaha, J. Cryst. Growth **311**, 4265 (2009).
35. J. M. McBride, Lecture at NORDITA Workshop "Origins of homochirality" (Feb. 2008) http://agenda.albanova.se/conferenceDisplay.py?confId=322
36. B. Kaptein, W. L. Noorduin, H. Meekes, W. J. P. van Enckevort, R. M. Kellogg, and E. Vlieg, Angew. Chem. Int. Ed. **47**, 1 (2008).